Au@MNPs-based electrochemical immunosensor for Vitamin D_3 serum samples analysis

Francesca Polli [a], Cristine D'Agostino [a], Rosaceleste Zumpano [a], Viviana De Martino[b], Gabriele Favero[c], Luciano Colangelo[b], Salvatore Minisola[b], Franco Mazzei [a]*

[a] Department of Chemistry and Drug Technologies, Sapienza University of Rome, P.le Aldo Moro 5, 00185 Rome, Italy

[b] Department of Clinical, Internal, Anaesthesiologic and Cardiovascular Sciences; Sapienza University of Rome, P.le Aldo Moro 5, 00185 Rome, Italy

[c] Department of Environmental Biology, Sapienza University of Rome, P.le Aldo Moro 5, Rome, Italy, 00185.

*Prof. Franco Mazzei: franco.mazzei@uniroma1.it; Tel.: +39-0649913225

Abstract

We report a new sensitive label-free electrochemical immunosensor to detect Vitamin D_3 (25-OHD_3) in untreated serum samples. To this aim, a graphite screen printed electrode (SPE) was modified using cysteamine (CYM) functionalized core-shell magnetic nanoparticles (Au@MNPs) then, the 25-OHD_3 antibody (AbD) was immobilized via glutaraldehyde crosslinking. The several steps involved in the immunosensor development and 25-OHD_3 analysis were monitored by using differential pulse voltammetry (DPV). The developed immunosensor showed a LOD of 2.4 ng/mL and a linear range between 7.4 – 70 ng/mL. The effectiveness of the immunosensor in human serum analysis was assessed by comparing the results obtained with the chemiluminescence-immunoassay (CLIA) reference method. The high sensitivity and excellent agreement with the reference method suggest its potential use as a POCT to monitor hypovitaminosis 25-OHD levels.

Keywords: Vitamin D_3 detection, gold-magnetic nanoparticles, label-free immunosensor, differential pulse voltammetry

1. Introduction

Vitamin D is one of the key determinants of bone and mineral metabolism, on which it exerts its main hormonal effects. Due to its complex metabolism, mechanisms of action, and the variety of cells and tissues expressing the specific receptor, vitamin D is involved in many metabolic pathways beyond the skeleton [1]. Under physiological conditions, active vitamin D i.e. 1,25-dihydroxy-vitamin D [1,25$(OH)_2$D] acts as a cofactor in the muscle, cardiovascular, pulmonary, skin, and immune system processes. Hypovitaminosis D is common in many health conditions associated with organs and systems [2]. Several epidemiological data have been published in the last decade, showing that Vitamin D deficiency was reported in a range of 7-90% of worldwide population with considerable variation observed between different countries and populations.[2]. The growing interest in vitamin D research and the need to recommend dietary reference intakes of vitamin D by regulatory agencies led to several controversial issues on the definition of hypovitaminosis D [3,4]. One of the main and most discussed point in this context is the definition of standardized methods to determine vitamin D status [4]. The accepted biomarker for the assessment of vitamin D status is 25-hydroxy-vitamin D [25-OHD] in serum, given its long half-life and higher metabolic stability in the circulation compared to other vitamin D metabolites [4]. Hence, the quality and standardization of 25-OHD assays are primary requisites in research studies to avoid

misclassifying vitamin D status. Standardization and quality programs developed internationally with this scope, and efforts were made to define reference procedures and materials. As per the standardized protocols, the analytical assessment of 25-OHD should exclude serum concentration of metabolites of vitamin D with physiological activity, such as 3-epi-25(OH)D_3, 24,25-dihydroxy vitamin D [24,25$(OH)_2D_3$], 1,25$(OH)_2D_3$ and 1,25$(OH)_2D_2$, whose cross-reactivity with 25-OHD may interfere with measurements. Additionally, serum circulating levels of a total 25-OHD include the concentration of both 25-OHD_3 and 25-OHD_2; this may represent an issue for the determination of vitamin D status in patients taking vitamin D_2 supplementation. Finally, patient-related confounders may interfere with the characteristics of the matrix, as seen during pregnancy or in osteoporosis or hemodialysis patients. The most reliable method for addressing all these issues is liquid chromatography coupled with tandem mass spectrometry (LC-MS/MS); it currently represents the gold reference standard method for 25-OHD measurement in research studies [4]. Contrary to LC-MS/MS, whose availability is limited to specialized centers, radioimmunoassay (RIA) methods for vitamin D assessment are the most commonly employed in clinical laboratories. The RIA assays use antibodies specifically binding vitamin D; the limitations of RIA include the cross-reactivity with some metabolites of vitamin D, particularly 24,25$(OH)_2D$, and possible interference of vitamin D binding protein concentration in the determination of total 25-OHD levels [4,5]. Another method used in clinical practice is the chemiluminescence-immunoassay (CLIA) which has the advantage of employing an automated analyzer, although cross-reactivity has been described, particularly with cholesterol and bilirubin [6]. Furthermore, both RIA and CLIA methods are time consuming and require specialized personnel. Notwithstanding these limitations, RIA and CLIA methods could be helpful in clinical practice to give an overall idea of vitamin D status and guide patients' management [7]. The increasing demand for fast and reliable methods to be used as POCTs to reduce the pressure on analysis laboratories and the costs of national health systems boosted the development of new analytical devices. Electrochemical biosensors can play a crucial role in this context, owing to their reduced cost, speed, sensitivity, and miniaturizability. Several works have been published concerning Vitamin D electrochemical detection in recent years often with interesting analytical performances but still far to be really considered as prototypes for POCT development. In 2013 our group published a comparison in the analysis of Vitamin D between an electrochemical immunosensor-based on 4-ferrocenylmethyl-1,2,4-triazoline-3,5-dione as a redox marker (detection limit of 10 ng/mL) and an SPR-based immunosensor (detection limit of 1 μg/mL) [6]. In that case, it has been shown that the electrochemical sensing technique behaved better than the surface plasmon resonance technique, thus encouraging further development of this type of transducer for Vitamin D biosensor. Several works on electrochemical methods to determine Vitamin D were successively published. Canevari et al. realized a glassy carbon modified electrode employing Nickel(II) hydroxide particles supported on silica and graphene hybrid material characterized by a detection limit of 3.26 nM [8]. Successively Ozbakir et al. published a work about a biosensor for 25-OHD_3 analysis by immobilizing the human cytochrome encoded by the gene P45027B1 on a glassy carbon electrode by using cobalt sepulchrate trichloride as a redox mediator in the cyclic and square wave voltammetry measurements [9]. Chauhan et al. in 2018, proposed an hydrolyzed Fe_3O_4/polyacrylonitrile fibers electrospun Indium Tin Oxide (ITO) electrode as a sensing electrode in the development of an immunosensor for the detection of 25-OHD_3. This electrochemical immunosensor showed a LOD of 0.12 ng/mL [10]. Successively, in 2019 Chauhan et al. realized an electrochemical immunosensor for Vitamin-D_3 detection based on aspartic acid-functionalized gadolinium oxide nanorods, with a detection limit of 0.10 ng/mL [11]. Kaur et al. In 2020 developed gold-platinum nanoparticles (Au-Pt NPs) supported on 3-(aminopropyl)triethoxysilane (APTES) modified Fluorine Tin Oxide (FTO) glass electrode as the transducer of an immunosensor for the detection of 25-OHD_3 (LOD of 0.49 pg/mL) [12].

In this work, we describe gold covered - magnetic nanoparticles (Au@MNPs)-based electrochemical immunosensors for the fast, simple, cheap, sensitive and accurate determination of vitamin D. The magnetic particles, in fact, together with

the use of magnetic support for electrodes, are able to help the reproducibility of the modification by dropcasting, avoiding coffe-ring effect [13]. This aspect plays a key role especially in the immunosensor development where the surface stability is one of the main issue to address. Moreover, the Au@MNPs can be easily purified, functionalized and manipulated thanks to magnetic separation. The Au@MNPs based immunosensor was then used to analyse the 25-OHD content in serum samples and the results were compared with those obtained with the chemiluminescent immunoassay (CLIA) reference method showing a good correlation.

2. Materials and methods

2.1. Materials

Au covered iron oxide nanoparticles (Au@MNPs) 25 mg/mL, solution were purchased from Micromod Partikeltechnologie GmbH (Germany). Cysteamine hydrochloride (CYM), glutaraldehyde 25% solution, sodium phosphate monobasic (NaH_2PO_4), Bovine serum albumin (BSA), sodium phosphate dibasic (Na_2HPO_4), potassium chloride (KCl), potassium ferricyanide trihydrate ($K_3[Fe(CN)_6]\cdot 3H_2O$), potassium ferrocyanide hexahydrate ($K_4[Fe(CN)_6]\cdot 6H_2O$), 2-(N-morpholino)ethanesulfonic acid (MES), 11-mercaptoundecanoic acid (MUA) and 3-mercaptopropionic acid (MPA) were obtained from Sigma Aldrich (St. Louis, MO, USA). 25-OHD_3 Recombinant Rabbit Monoclonal Antibody (AbD) antibody by Thermo Fisher Scientific Inc. (MA, USA) were stored at -20°C in aliquots of 30 µg/mL in 20 mM PBS buffer pH 7.4 to avoid repeated freeze and thaw cycles. LIAISON® 25-OHD TOTAL for chemiluminescent immunoassay (CLIA) technology for the quantitative determination of 25-OHD in human serum was obtained from DiaSorin (Vicenza, Italy). Human serum samples, collected from voluntary donors under 25-OHD_3 treatment, were provided by Prof. Salvatore Minisola Laboratory (Rome, Italy). 25-OHD_3 was purchased from Gentaur GmbH (Germany). The samples were stored at -80°C and tested without further dilution. All solutions were prepared using Milli-Q water (18.2 MΩ cm, Millipore, Bedford, MA, USA). The magnetic rack for magnetic separation was purchased from Ademtech (France), while the rotating agitator (25rad/s) was developed from the Mechanical Engineering Department of Sapienza University of Rome (Italy). Graphite screen printed electrodes (DRP-110), gold electrode classic (Au-TIP), and magnetic support for drop-casting and measurement were obtained by Metrohm (Switzerland)

2.2. Au@MNPs functionalization

Before using, 10 µL of Au@MNPs nanoparticles suspension were diluted in 490 µL of distilled water and separated in a magnetic rack for 2 minutes, removing the supernatant [14]. The procedure was repeated twice, and the solution turned from dark to light brown at the end of the process. After washing, Au@MNPs were incubated for 2 hours in a rotating agitator 500 µL with a freshly prepared 18 mM CYM in 10 mM PBS to limit the thiol group's deprotonation responsible for the collateral disulfide formation [15,16] and the functionalization was assessed by means of FT-IR and Raman spectroscopy (Supporting Material Figure S1 and S2). Moreover, during the whole functionalization process, the solution was kept in the dark to prevent the oxidation of thiols from UV light through the radical path [17]. The MPA@AuMNPs were obtained with the same procedure by incubating the washed AuMNPs in a 2 mM MPA solution while the MUA@AuMNPs were functionalized in a 1 mM MUA solution.

2.3. Electrode preparation

The graphite electrodes were gently rinsed with distilled water, and 15 µL of a CYM@AuMNPs solution were drop-cast onto the working electrode. The modified nanoparticles solution was left to dry at room temperature under a fume hood. The SPE (Screen Printed Electrode) was placed on magnetic support before the washing step to avoid any loss of nanomaterial. Once the surface was dried, the amino groups of CYM were activated by treating the surface with 15 µL of a 10% glutaraldehyde solution for 10 minutes and then rinsed with water. This time and concentration combination allows to carry out the reaction with amino groups without the occurrence of polymerization reaction [18,19]. 15 µL of a 30 µg/mL AbD solution were then dropped on the electrode and left to react for 30 minutes. The surface was washed with PBS and left to stabilize for 18h in a humidity chamber at 4°C in the fridge. The electrodes were then deactivated by treating with 10 µg/mL bovine serum albumin solution in PBS for 20 minutes to avoid nonspecific adsorption. All the steps involved in the SPE modification have been characterized by using FT-IR and Raman spectroscopy (Supporting Material, Figur S1 and S2).

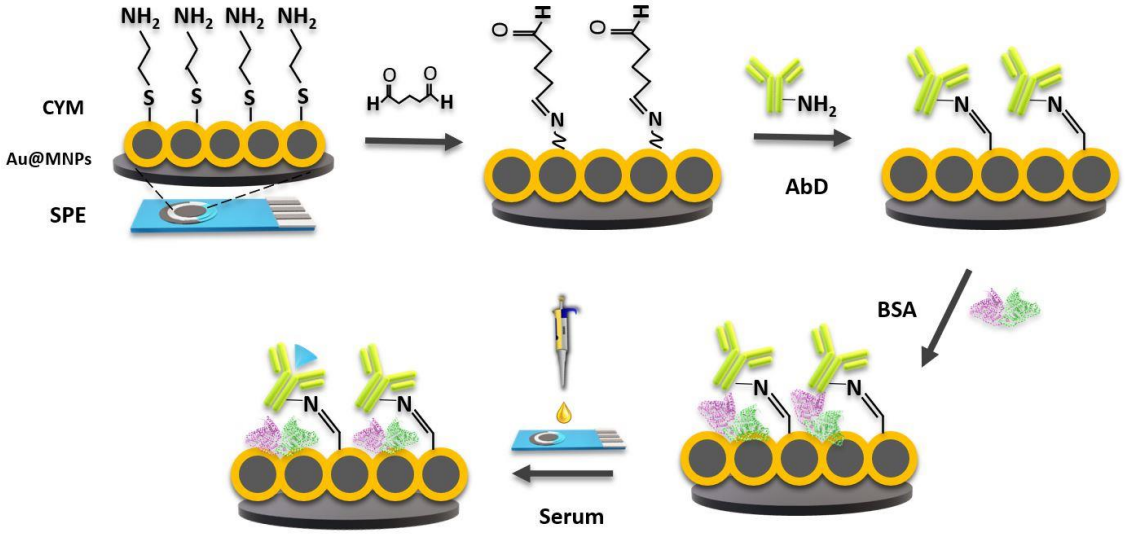

Fig. 1. Scheme of assembly of the AuMNPs-based immunosensor with Ab immobilization via glutaraldehyde crosslinking.

2.4. DPV calibration of 25-OHD

The immunosensor calibration was obtained after treating the electrodes with 25-OHD standard solutions in the range 7.4 – 70.0 ng/mL. The signal was recorded with a potentiostat using the DPV technique. To this aim, 15 µL of the standard solution were incubated for 30 minutes at room temperature. Then, the excess was removed by washing the electrode with PBS buffer. Before doing the DPV measurements, the electrode can be removed from their magnetic support, and the DPV measurements were carried out with a 1.1 mM $[Fe(CN)_6]^{3-/4-}$,100 mM KCl solution between [-0.4 ; 0.6] V.

2.5 Specificity studies

Specificity studies has been carried out by incubating the SPE/CYM@AuMNPs/AbD/BSA modified electrodes with 15 µL of the same amount of 25-OHD_3 solutions containing one of several given serum interferents: 4.0 mM glucose, 1.0 mM oxalic acid, 4 mM glycine, 0.1 mM ascorbic acid and urea 4 mM. Moreover, to better understand the real ability of the sensor to work in such conditions, 25-OHD_3 content of each interferent concentration was kept at 8 ng/mL, near the LOQ, in order to highlight the interferents effect if present.

2.6 Electrochemical measurements

Electrochemical signal of the different modified electrodes was followed by DPV and EIS measurements and the concentration of the probe was accurately chosen on the basis of the procedure according to the literature [20] and to have a better resolution during the characterization of each step of the immunosensor development. To this aim, a solution 5 mM of $[Fe(CN)_6]^{3-/4-}$, 100 mM KCl was used for EIS measurements to check the modification on a SAM modified surface. For DPV measurements a concentration of 1.1 mM $[Fe(CN)_6]^{3-/4-}$, 100 mM KCl has been used, and the potential was investigated between [-0.4 to + 0.6] V vs Ag|AgCl at 10 mV/s using a step potential of 5 mV.

Furthermore, a preliminary evaluation of the electrochemical performances of the three different functionalization was also repeated increasing the probe concentration to 2 mM to highlight the differences of charge transfer between the batches of CYM@AuMNPs, MPA@AuMNPs and MUA@AuMNPs. EIS measurements were performed in a frequency range between 10 000 and 0.1 Hz and 5 mV amplitude in order to follow each modification step. The measurements were performed in a three electrode electrochemical cell using an Ag/AgCl as a Reference electrode and a graphite counter electrode. The gold working electrode was modified with MPA 2 mM solution (4h in ethanol). The carboxylic groups of the thiol were then activated by EDC/NHS to react with the amino groups of 30 μg/mL of AbD. The Au/MPA/AbD electrodes were then treated with a solution of 1 ng/mL of 25-OHD_3.

3. Results and discussion

3.1 Capping agent influence on DPV

The electrochemical immunosensor was developed as schematically shown in **Fig. 1**. Au@MNPs were washed by magnetic separation and then functionalized by ligand-exchange incubating in three different thiols solutions: CYM, MPA and MUA Before the functionalization, the pH was adjusted to maintain the capping agent's ionization but without maximizing the ionic strength to avoid Au@MNPs aggregation occurring by the counter-ions effect on Zeta potential [21]. To this aim, a KOH dilute solution was used to increase the double layer thickness reducing the precipitation phenomenon [22]. The three batches of thiol functionalized Au@MNPs were tested by DPV. In **Fig.2(A)** he DPV curves obtained for citrate capped Au@MNPs (as obtained by the producer) are compared to those obtained with MPA and CYM capped ones;it is highlighted how the functionalization with CYM provides a higher signal increase with respect to MPA functionalized AuMNPs. On the contrary the lower signal in absence of thiols functionalization is obtained in the presence of the citrate stabilizing agent of the commercial batch.

This result can be attributed to repulsion between the negative probe $[Fe(CN)_6]^{3-/4-}$ and the carboxylic groups exposed on the MPA@AuMNPs modified surface [23]. This repulsion increases when the number of charged residues passes from one (of MPA@AuMNPs) to three (of Citrate@AuMNPs) of the commercial AuMNPs. Moreover, in **Fig.2B** a further current decrease was recorded by functionalizing the surface with a negative thiol with a higher chain length. In fact, MUA@AuMNPs are reported to obstacle the diffusion of the probe through the hydrophobic undecanoic chain [21,24] more than commercial AuMNPs. This consideration makes positive and short thiols like CYM the very performing capping agent for DPV immunosensor development. Different CYM concentrations were then tested to both maximize and stabilize the Au@MNPs solution **(Fig.2C)** and the best one was used for the functionalization procedure.

In order to optimize the amount of deposited Au@MNPs, a dilution of 1:50 was chosen on the basis of the volume and the concentration of the commercial Au@MNPs batch to guarantee a complete coverage of the electrode surface. These amino-functionalized nanoparticles show a particular stability when absorbed on graphite, and once dried, they don't detach even after several steps of thoroughly rinsing. The same electrochemical signal was detected before and after

several washing steps. The good adhesion between the Au@MNPs and the electrode increases the reproducibility of the following modifications thanks to the electrostatic interaction between positive groups of CYM and graphite π delocalized orbitals. Furthermore, the magnet localized below the WE helps the Au@MNPs to be homogenously distributed on the surface, simultaneously avoiding the "coffee ring" effect. [13,25].

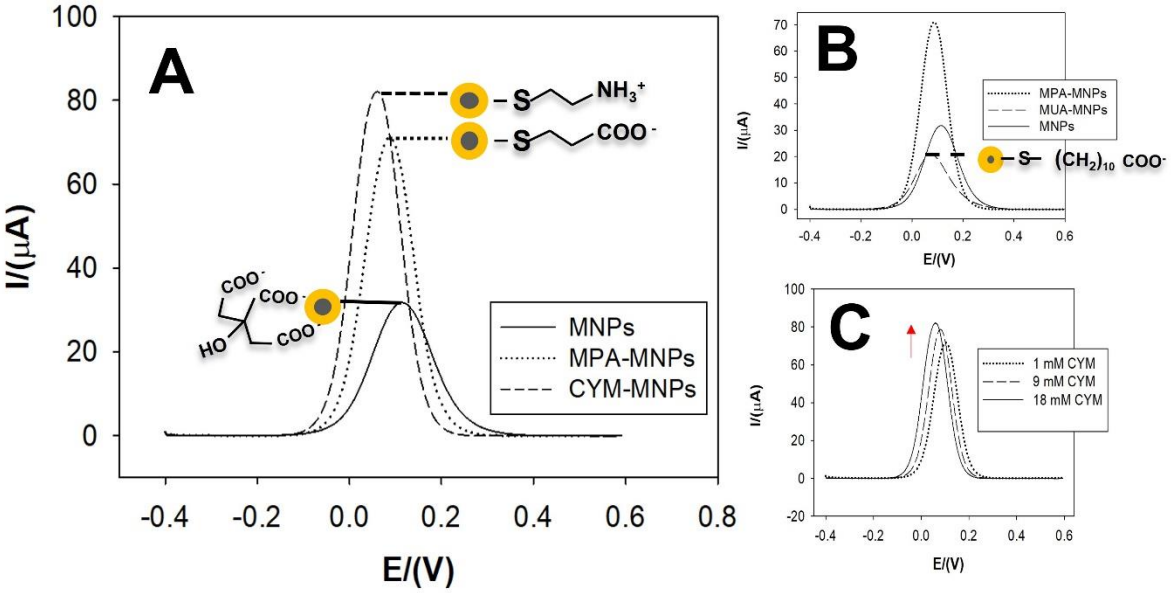

Fig.2. DPV of SPE graphite electrode modified with: (A) CYMAu@MNPs , MPA@AuMNPs and commercial Citrate@AuMNPs (B) MPA@AuMNPs and MUA@AuMNPs amd (C) CYM@AuMNPs functionalized by different CYM concentrations.

3.2. Antibody immobilization

DPV measurements were also employed to characterize and optimize the antibody immobilization step and the influence of AbD loading on the 25-OHD_3 detection was evaluated as well (Supporting Material, Fig. S7). In **Fig.3(A)** are reported the different DPV peak lead after AbD immobilization on CYM@AuMNPs via glutaraldehyde cross-linking and the following interaction with the antigen. It's interesting to see that the same modifications didn't leads to the same signal decrease when applied to a MPA@AuMNPs modified electrode. As shown in Fig. 3(B), CYM capped Au@MNPs can increase the amount of Ab immobilized compared to that obtained with MPA capped ones. These results can be explained by considering some particular aspects concerning IgGs' charge distribution and the relationship between protein density and the IgG orientation on a solid substrate. As reported in the literature, in fact, IgG's molecule is composed by two fragments: the part able to interact with the antigen - known as $(Fab)_2$ fragment - and the so-called "crystallizable fragment" (Fc) deputed to interact with cells that mediate the immune response [26]. The chemical immobilization of an antibody on a solid substrate generally happens randomly when a site-direct method is not adopted, with the equal probability of both fragments keeping in touch with the surface, thus reducing the sensing surface's ability to bind the antigen [14,27–29]. However, some little precautions can be adopted. In fact, as well established, because of the abundance of basic residues in the $(Fab)_2$ region, the whole IgG's dipolar moment is pointing from Fc to the $(Fab)_2$ fragment. This aspect makes the immobilization of Abs on negative surfaces particularly unfavorable for its correct orientation and at the same time much more susceptible to pH's variations.

As well described by the work of Lou et al. [30] and by Montecarlo simulations of Zhou et al. [31], when using pH around 7.8, the presence of a negative net charge in the Fc region and a positive charge on the $(Fab)_2$ makes a high number of IgG molecules approaching to the surface in the "head-on" configuration, with the $(Fab)_2$ sticked to the surface and thus unable to bind the antigen. The repulsion between Fc and the surface and its attraction with $(Fab)_2$, in cited works, is lowered by leading the immobilization step in acidic condition. In this work, the use of positive charged nanoparticles can mitigate the pH-dependent interaction between the IgG and the surface, allowing the operator to choose the pH on the basis of the chemical reaction to be employed.

Moreover, as shown in the work of Buji et al.[32] and in other site-directed immobilization strategies, a vertical Ab orientation generally involves a higher amount of Ab that the surface can host [27,29,30,32]. Based on the Fc and Fab_2 crystallized structure, the predicted antibody end-on arrangement can reach a medium protein density of around 3.7 ng/mm^2 instead of 2.0 ng/mm^2 obtained when Ab is arranged in side-on and lying-on configurations [32]. For these reasons, i.e. the electrostatic attraction driving the orientation of immobilization, the use of CYM may involve a higher amount of Ab immobilized in effective orientation and can be detected by DPV as a higher signal decrease in Fig. 3.

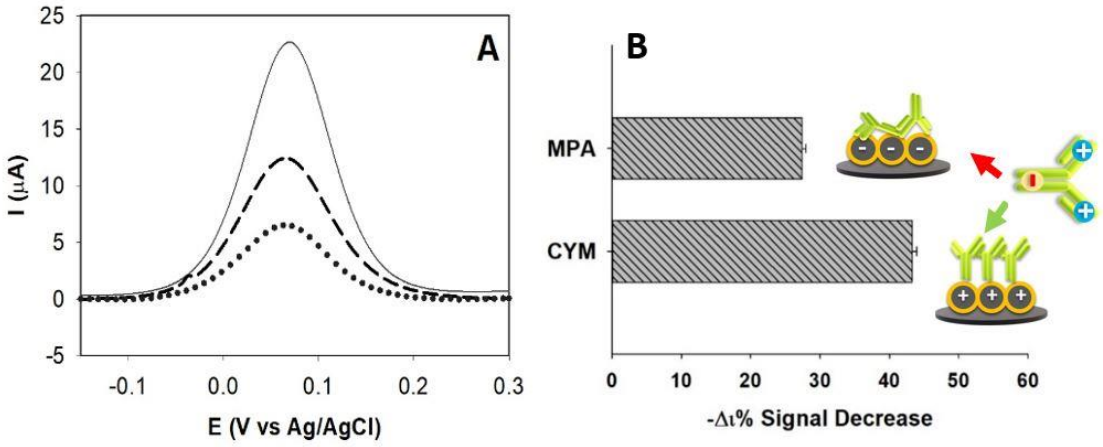

Fig.3. (A) DPV characterization of 25-OHD_3 interaction (dotted line) and AbD immobilization (dashed line) on a CYM@AuMNPs (solid line). (B) Signal decreasing recorded after the Ab immobilization on CYM and MPA functionalized Au@MNPs.

3.3 EIS measurements

To better characterize the physico-chemical changes induced on an electrode surface after 25-OHD_3 binding, a simple platform was designed in order to evaluate and isolate the 25-OHD_3 contribution to the charge transfer resistance. To this aim, the molecule was left to interact 30 minutes with a AbD modified electrodes and the Rct increasing was followed by running EIS measurements [33].The results reported in the Nyquist plot were fitted by using the Randles' circuit [34] reported in the figure's inset (**Fig.4**). As reported in **Table 1**, the incubation of a low concentration of 25-OHD_3 on a AbD/MPA/Au electrode leads to a Rct increase of almost the 54% with the R_{ct} value passing from 2.20 kΩ to 3.38 kΩ in the absence and in the presence of 1 ng/mL of 25-OHD_3 respectively. The high resistance measured as a consequence of 25-OHD_3 -Ab interaction, can't be explained only on the basis of the steric hindrance gained after the binding. In fact, as reported by Deb et al [35], the 25-OHD and their derivatives have a rather low molecular weight ranging from about 360.54 to 446.63 g/mol, which can justify only in part the huge difference detected in the Rct value obtained before and after antigen interaction [35–37]. Indeed, another important factor to consider is that 25(OH)D is categorized among the

fat-soluble vitamins and, with its metabolites, shows predicted log P values between 3.0 (for the most hydroxylated forms such as 1,23S,25-trihydroxy-24-oxo-vitamin D_3) to 9.02 for the less metabolized ones [35,38]. This means that Vitamin D and related metabolites, rather hydrophobic compounds, are likely to create an obstacle to the diffusion of polar species towards the electrode surface.

In particular, 25-OHD_3 form has a log P of 8.8 and low solubility in water [35]; this characteristic may obstacle the diffusion of the hydrophilic probe used in our measurements ($[Fe(CN)_6]^{3-/4-}$) to reach the surface and discharge more abundantly than hydrophilic molecules with the same molecular weight.

The synergic action due to both the intrinsic lipophilic nature of 25-OHD_3 and the steric hindrance occurring after antigen binding, amplify the current decrease. Therefore, the electrochemical label-free approach could be particularly useful for the development of a sensitive immunosensors towards 25-OHD_3, especially if coupled with techniques that can be supported by portable systems, such as DPV. Based on this findings, among all the electrochemical techniques, DPV was employed for this label-free immunosensor development.

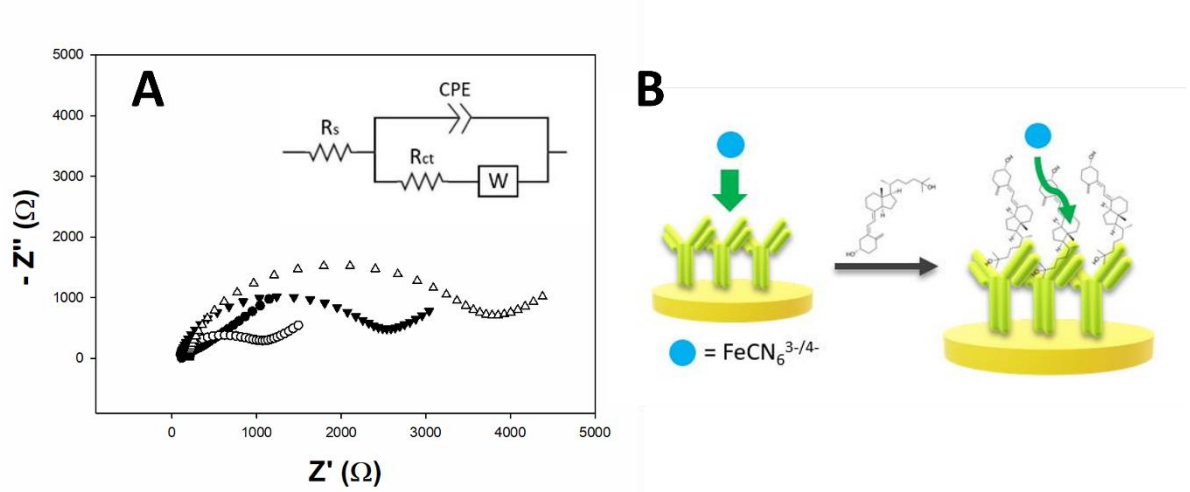

Fig.4 (**A**) Nquist plot of Au Bare (black dots) electrode, MPA/Au (white dots), AbD/MPA/Au (black triangles) and 25-OHD_3 /AbD/MPA/Au (white triangles) with 25-OHD_3 at a 1ng/mL. (**B**) Scheme of assembly of EIS measurements.

Modification	R_{ct} (kΩ)
Au (Bare)	0,08
Au/MPA	0,93
Au/MPA/Ab/BSA	2,20
Au/MPA/Ab/BSA/25-OHD3	3,38

Table.1 R_{ct} values obtained for Nquist plot in Fig.4 (A).

3.4 Calibration and CLIA correlation

The developed immunosensor was calibrated using 25(OH)D LYASION standard solutions and the DPV curves were obtained. As shown in **Fig. 5A** a peak decrease was revealed at increasing 25-OHD concentration. The calibration curve obtained in **Fig.5C** shows a high sensitivity, a linearity range and a LOD value (calculated as three times the blank's SD and dividing the result for the slope) that together makes it a suitable tool to perform clinical analysis. The method was

then validated with the CLIA method by analyzing human serum samples. For this aim 11 samples, were collected at different times by people under pharmacological treatment for hypovitaminosis comparing the results with those obtained with the chemiluminescent immunoassay (CLIA) standard reference method [39]. As reported in **Table 2** the 25-OHD_3 concentration determined by the immunosensor showed a good agreement with the CLIA reference method (**Fig.5E**) and exhibits a correlation coefficient of 0.980, with a recovery between ~ 95 and 107 %. The electrochemical method has shown a good reproducibility with a medium SD of ± 0,16 μA (**Fig.5B**) and the capability to maintain the 97% of the signal after being stored for 6 days at 4°C (Supplementary Material, Fig. S6). As a further test, the ability to detect 25-OHD_3 in the presence of serum interferents was tested (**Fig.5D**) and the results showed a substantial absence of signal disruption taking into account the good agreement of peak intensity obtained in presence and in absence of interfering species, thus confirming the great capability of the sensor to work in real matrix with no significant signal change occurring.

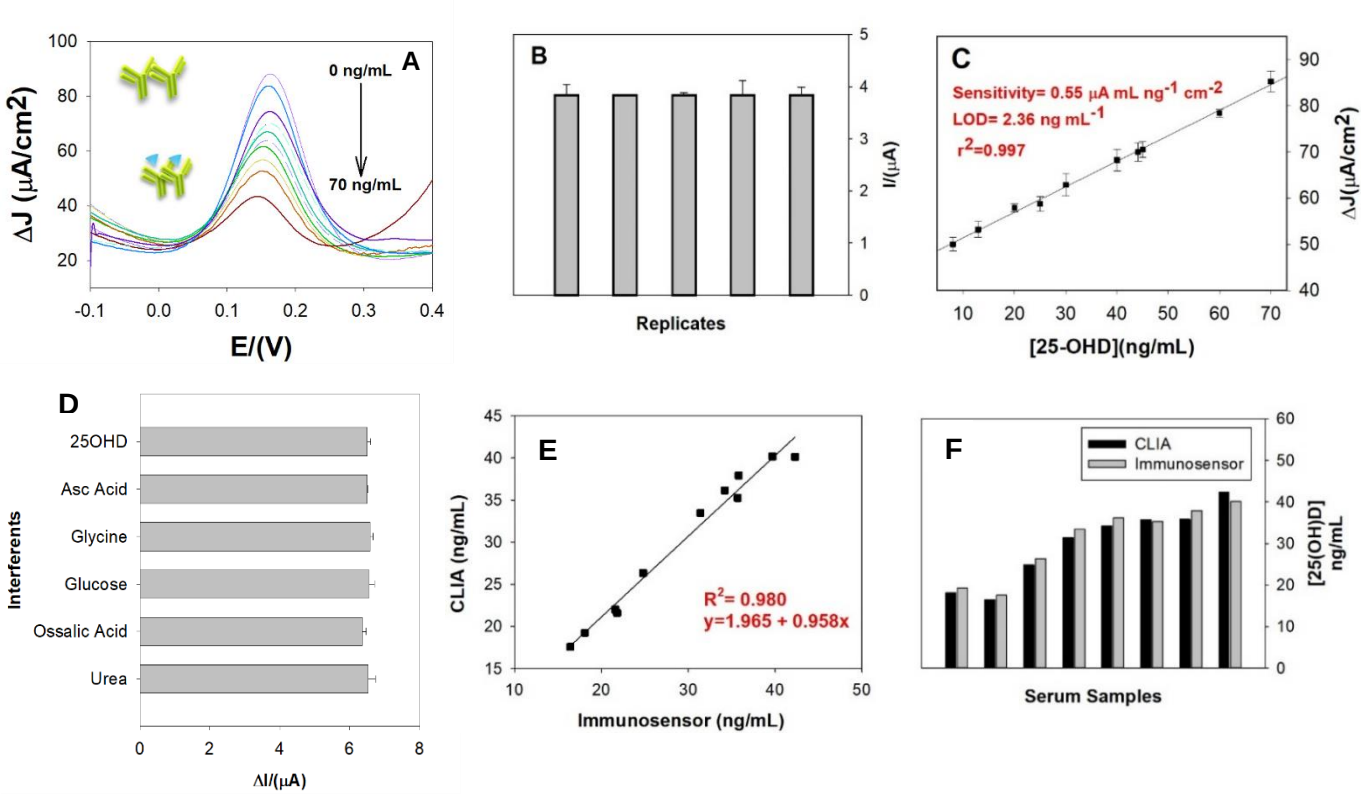

Fig.5. (**A**) Differential pulse voltammograms of SPE/CYM@AuMNPs/AbD/BSA modified electrodes obtained after 30 minutes incubation with increasing 25-OHD_3 concentrations. (**B**) Reproducibility of the sample (35.80 ng/mL). (**C**) Sensor calibration obtained after incubation of 25-OHD standard solutions from LIAISON™ kit (**D**) Signal obtained after 25-OHD_3 alone and in presence of different interferents species (**E**) Correlation between 25(OH)D_3 concentration for human samples tested (1-11) with the Au@MNPs electrochemical method and the CLIA reference method. (**F**) Comparison of 25-OHD_3 concentrations found with CLIA and with the DPV immunosensor.

As reported in **Table 3**, this fabricated immunosensor shows a LOD of 2.36 ng/mL and a linearity range between 7.4 and 70 ng/mL that covers the whole clinical range required, unlike many previous works for 25-OHD_3 detection without a previous dilution. Moreover, the coupling between these features with the achievement of one of the higher sensitivities reported so far, makes it a suitable tool not just to monitor with accuracy 25-OHD levels even in patients with severe hypovitaminosis, but also to follow even small 25-OHD variations during the treatment. In fact, this work shows, together with the work of Chauhan et al.[10], the most performing combination between sensitivity, linear range and LOD values among the 25-OHD_3 sensors available in the literature, but does not require an adhesion material between the electrode and the magnetic nanoparticles thanks to an accurate selection of the capping agent in a way to provide good electrostatic interaction with the graphite substrate. Furthermore, another improvement that could have played a role in the sensitivity obtained could be the use of a positively charged surface that can prevent the wrong antibody orientation to the surface

that can occur due to the Ab isoelectric point. Another key aspect of our research to point out is the high number of serum samples studied, in fact, between 25-OHD reported sensors (**Table 3)**, the serum samples analysis has been carried out for only two out of eight works (Cys-Au@ZrO_2/ITO LOD =3.54 ng ml^{-1} and $nCeO_2$/ITO LOD = 4.63 ng ml^{-1}) and, in addition, considering no more than 5 samples. Therefore, for the best of our knowledge, our work presents the higher number of serum samples analyzed than any other experimental electrochemical immunosensor available in literature and, among the validated ones, the one exhibiting the lower limit of detection.

CLIA (ng/mL)	**Immunosensor** (ng/mL)	**RSD** (%)	**Recovery** (%)
34.2	36.16	2.55	105.7
35.7	35.25	5.27	98.7
35.8	37.92	4.21	105.9
18.1	19.25	3.55	106.4
16.4	17.56	3.86	107.1
24.8	26.34	1.96	106.2
31.4	33.48	2.93	106.6
21.8	21.61	6.52	99.11
21.6	22.00	5.13	101.8
21.4	22.78	2.30	106.4
42.3	40.13	3.66	94.91

Table 2. Recovery and RSD values for CYM@AuMNPs immunosensor of the 11 serum samples.

Immunosensor	**Technique**	**Linearity Range**	**LOD**	**Sensitivity**	**Ref.**
MUA/AuNPs	SPR	5–50 μg ml^{-1}	1 μg ml^{-1}	4.8 m°ml μg^{-1}	[6]
MPA/Au	DPV	20–200 ng ml^{-1}	10 ng ml^{-1}	0.16 μA ml ng^{-1} cm^{-2}	[6]
CAEF/RCP*	Chrono-amperometry	10 – 100 ng ml^{-1}	10 ng ml^{-1}	0.16 μA ml ng^{-1} cm^{-2}	[40]
$nCeO_2$/CC**	DPV	1– 200 ng ml^{-1}	4.63 ng ml^{-1}	2.08 μA ml ng^{-1} cm^{-2}	[41]
Cys-Au@ZrO2/ITO	DPV	1–50 ng ml^{-1}	3.54 ng ml^{-1}	2.01 μA ml ng^{-1} cm^{-2}	[42]
CD-CH*/ITO**	DPV	10–50 ng ml^{-1}	1.35 ng ml^{-1}	0.2 μA ml ng^{-1} cm^{-2}	[43]
Asp-Gd_2O_3NRs/ITO	DPV	10–100 ng ml^{-1}	0.10 ng ml^{-1}	0.38 μA ml ng^{-1} cm^{-2}	[11]
Fe_3O_4-PANnFs/ITO	DPV	10–100 ng ml^{-1}	0.12 ng ml^{-1}	0.90 μA ml ng^{-1} cm^{-2}	[10]
CYM@AuMNPs	DPV	7.4 – 70 ng ml^{-1}	2.4 ng ml^{-1}	0.55 μA ml ng^{-1} cm^{-2}	**Present work**

Table 3. Summary of analytical performances of 25-OHD immunosensors. CAEF/RCP* (electrospun cellulose acetate fibers). $nCeO_2$/CC** (cerium oxide nanoparticles modified carbon cloth). CD-CH*** (Carbon dots modified with chitosan).

4. Conclusions

In this work, we developed an electrochemical label-free immunosensor for detecting 25-OHD_3. To this aim, we optimized the experimental procedures for Cysteamine functionalized-gold magnetic nanoparticles to modify graphite-SPE electrode surfaces to allow the site-directed immobilization of antibodies, thus improving the performance of the resulting immunosensor. The developed immunosensor has shown good reproducibility with an average SD of ± 0,16 µA and the capability to maintain the 97% of the signal after being stored for 6 days at 4°C. Furthermore, the immunosensor displayed a LOD of 2.36 ng/mL and a linearity range between 7.4 and 70 ng/mL covering the clinical range required for hypovitaminosis diagnosis, unlike many previous works reported in the literature. The results obtained with the developed immunosensor in the analysis of 11 human serum samples, collected at different times by people under pharmacological treatment for hypovitaminosis, were compared with those obtained with the chemiluminescent immunoassay (CLIA) standard reference method showing a good agreement. The high sensitivity and excellent agreement with the reference method suggest the potential use of the developed immunosensor as a POCT to monitor hypovitaminosis 25-OHD levels.

Acknowledgements

This work was granted by Regione Lazio project entitled "NanoBioPOCT25-OHD" - Progetti Gruppi di Ricerca Conoscenza e Cooperazione per un Nuovo Modello di Sviluppo

Conflict of interest

The authors declare no conflict of interest.

Appendix A. Supplementary Materials

5. References

[1] R. Bouillon, Extra-Skeletal Effects of Vitamin D, Front. Horm. Res. 50 (2018) 72–88. https://doi.org/10.1159/000486072.

[2] A. Giustina, R. Bouillon, N. Binkley, C. Sempos, R.A. Adler, J. Bollerslev, B. Dawson-Hughes, P.R. Ebeling, D. Feldman, A. Heijboer, G. Jones, C.S. Kovacs, M. Lazaretti-Castro, P. Lips, C. Marcocci, S. Minisola, N. Napoli, R. Rizzoli, R. Scragg, J.H. White, A.M. Formenti, J.P. Bilezikian, Controversies in Vitamin D: A Statement From the Third International Conference., JBMR Plus. 4 (2020) e10417. https://doi.org/10.1002/jbm4.10417.

[3] A.C. Ross, C.L. Taylor, A.L. Yaktine, H.B. Del, Dietary Reference Intakes for Calcium and Vitamin D, 2011. https://doi.org/10.17226/13050.

[4] C.T. Sempos, A.C. Heijboer, D.D. Bikle, J. Bollerslev, R. Bouillon, P.M. Brannon, H.F. DeLuca, G. Jones, C.F. Munns, J.P. Bilezikian, A. Giustina, N. Binkley, Vitamin D assays and the definition of hypovitaminosis D: results from the First International Conference on Controversies in Vitamin D., Br. J. Clin. Pharmacol. 84 (2018) 2194–2207. https://doi.org/10.1111/bcp.13652.

[5] F. Ferrone, J. Pepe, V.C. Danese, V. Fassino, V. Cecchetti, F. De Lucia, F. Biamonte, L. Colangelo, G. Ferrazza, E. Panzini, A. Scillitani, L. Nieddu, F. Blocki, S.D. Rao, S. Minisola, C. Cipriani, The relative

influence of serum ionized calcium and 25-hydroxyvitamin D in regulating PTH secretion in healthy subjects., Bone. 125 (2019) 200–206. https://doi.org/10.1016/j.bone.2019.05.029.

[6] L. Carlucci, G. Favero, C. Tortolini, M. Di Fusco, E. Romagnoli, S. Minisola, F. Mazzei, Several approaches for vitamin D determination by surface plasmon resonance and electrochemical affinity biosensors, Biosens. Bioelectron. 40 (2013) 350–355. https://doi.org/10.1016/j.bios.2012.07.077.

[7] S. Minisola, L. Colangelo, C. Cipriani, J. Pepe, D.P. Cook, C. Mathieu, Screening for hypovitaminosis D: cost-effective or not?, Eur. J. Endocrinol. 180 (2019) D1–D7. https://doi.org/10.1530/EJE-18-0977.

[8] T. Canevari, F. Cincotto, R. Landers, S.A.. Machado, Synthesis and characterization of a-nickel (II) hydroxide particles on organic-inorganic matrix and its application in a sensitive electrochemical sensor for vitamin D determination, Electrochim. Acta. 147 (2014). https://doi.org/10.1016/j.electacta.2014.10.012.

[9] H. F Ozbakir, D. A Sambade, Detection of 25-Hydroxyvitamin D3 with an Enzyme modified Electrode, J. Biosens. Bioelectron. 07 (2016). https://doi.org/10.4172/2155-6210.1000193.

[10] D. Chauhan, P.K. Gupta, P.R. Solanki, Electrochemical immunosensor based on magnetite nanoparticles incorporated electrospun polyacrylonitrile nanofibers for Vitamin-D3 detection, Mater. Sci. Eng. C. 93 (2018) 145–156. https://doi.org/10.1016/j.msec.2018.07.036.

[11] D. Chauhan, R. Kumar, A.K. Panda, P.R. Solanki, An efficient electrochemical biosensor for Vitamin-D3 detection based on aspartic acid functionalized gadolinium oxide nanorods, J. Mater. Res. Technol. 8 (2019) 5490–5503. https://doi.org/10.1016/j.jmrt.2019.09.017.

[12] A. Kaur, S. Kapoor, A. Bharti, S. Rana, G. Chaudhary, N. Prabhakar, Gold-platinum bimetallic nanoparticles coated 3-(aminopropyl)triethoxysilane (APTES) based electrochemical immunosensor for vitamin D estimation, J. Electroanal. Chem. 873 (2020) 114400. https://doi.org/10.1016/j.jelechem.2020.114400.

[13] A. Kaliyaraj Selva Kumar, Y. Zhang, D. Li, R.G. Compton, A mini-review: How reliable is the drop casting technique?, Electrochem. Commun. 121 (2020) 106867. https://doi.org/10.1016/j.elecom.2020.106867.

[14] R. Zumpano, M. Manghisi, F. Polli, C. D'Agostino, F. Ietto, G. Favero, F. Mazzei, Label-free magnetic nanoparticles-based electrochemical immunosensor for atrazine detection, Anal. Bioanal. Chem. (2022). https://doi.org/10.1007/s00216-021-03838-y.

[15] X. Li, 乳鼠心肌提取 HHS Public Access, Physiol. Behav. 176 (2016) 139–148. https://doi.org/10.1016/j.freeradbiomed.2014.11.013.The.

[16] R. Zumpano, F. Polli, C.D. Agostino, R. Antiochia, G. Favero, Nanostructured-based electrochemical immunosensors as a diagnostic tool, (2020) 1–24.

[17] N. Feillée, M. De Fina, A. Ponche, C. Vaulot, S. Rigolet, L. Jacomine, H. Majjad, C. Ley, A. Chemtob, Step-growth thiol–thiol photopolymerization as radiation curing technology, J. Polym. Sci. Part A Polym. Chem. 55 (2017) 117–128. https://doi.org/10.1002/pola.28369.

[18] D.T. Cheung, N. Perelman, E.C. Ko, M.E. Nimni, Mechanism of crosslinking of proteins by glutaraldehyde III. Reaction with collagen in tissues, Connect. Tissue Res. 13 (1985) 109–115. https://doi.org/10.3109/03008208509152389.

[19] K. Okuda, I. Urabe, Y. Yamada, H. Okada, Reaction of glutaraldehyde with amino and thiol compounds, J. Ferment. Bioeng. 71 (1991) 100–105. https://doi.org/10.1016/0922-338X(91)90231-5.

[20] L. Chen, J. Jiang, G. Shen, R. Yu, A label-free electrochemical impedance immunosensor for the sensitive detection of aflatoxin B1, Anal. Methods. 7 (2015) 2354–2359. https://doi.org/10.1039/C4AY01981D.

[21] S.M. Ansar, S. Chakraborty, C.L. Kitchens, pH-responsive mercaptoundecanoic acid functionalized gold nanoparticles and applications in catalysis, Nanomaterials. 8 (2018) 1–12. https://doi.org/10.3390/nano8050339.

[22] T. Laaksonen, P. Ahonen, C. Johans, K. Kontturi, Stability and electrostatics of mercaptoundecanoic acid-capped gold nanoparticles with varying counterion size, ChemPhysChem. 7 (2006) 2143–2149. https://doi.org/10.1002/cphc.200600307.

[23] R. Javed, M. Zia, S. Naz, S.O. Aisida, N. ul Ain, Q. Ao, Role of capping agents in the application of nanoparticles in biomedicine and environmental remediation: recent trends and future prospects, J. Nanobiotechnology. 18 (2020) 1–15. https://doi.org/10.1186/s12951-020-00704-4.

[24] I. Fratoddi, Hydrophobic and Hydrophilic Au and Ag Nanoparticles. Breakthroughs and Perspectives., Nanomater. (Basel, Switzerland). 8 (2017). https://doi.org/10.3390/nano8010011.

[25] V. Poulichet, M. Morel, S. Rudiuk, D. Baigl, V. Poulichet, M. Morel, S. Rudiuk, D.B. Liquid-liquid, Liquid-liquid coffee-ring effect To cite this version : HAL Id : hal-03020973 Liquid-liquid coffee-ring effect, (2020) 370–375.

[26] P. Ghisellini, M. Caiazzo, A. Alessandrini, R. Eggenhöffner, M. Vassalli, P. Facci, Direct electrical control of IgG conformation and functional activity at surfaces, Sci. Rep. 6 (2016) 3–10. https://doi.org/10.1038/srep37779.

[27] D. Quaglio, F. Polli, C. Del Plato, G. Cianfoni, C. Tortora, F. Mazzei, B. Botta, A. Calcaterra, F. Ghirga, Calixarene: a versatile scaffold for the development of highly sensitive biosensors, Supramol. Chem. 00 (2021) 1–25. https://doi.org/10.1080/10610278.2021.2011283.

[28] D. Quaglio, L. Mangiardi, G. Venditti, C. Del Plato, F. Polli, F. Ghirga, G. Favero, M. Pierini, B. Botta, F. Mazzei, Site-Directed Antibody Immobilization by Resorc[4]arene-Based Immunosensors, Chem. - A Eur. J. 26 (2020) 8400–8406. https://doi.org/10.1002/chem.202000989.

[29] E. Capecchi, D. Piccinino, E. Tomaino, B.M. Bizzarri, F. Polli, R. Antiochia, F. Mazzei, R. Saladino, Lignin nanoparticles are renewable and functional platforms for the concanavalin a oriented immobilization of glucose oxidase-peroxidase in cascade bio-sensing, RSC Adv. 10 (2020) 29031–29042. https://doi.org/10.1039/d0ra04485g.

[30] D. Lou, L. Ji, L. Fan, Y. Ji, N. Gu, Y. Zhang, Antibody-Oriented Strategy and Mechanism for the Preparation of Fluorescent Nanoprobes for Fast and Sensitive Immunodetection, Langmuir. 35 (2019) 4860–4867. https://doi.org/10.1021/acs.langmuir.9b00150.

[31] J. Zhou, H.K. Tsao, Y.J. Sheng, S. Jiang, Monte Carlo simulations of antibody adsorption and orientation on charged surfaces, J. Chem. Phys. 121 (2004) 1050–1057. https://doi.org/10.1063/1.1757434.

[32] J. Buijs, J.W.T. Lichtenbelt, W. Norde, J. Lyklema, Adsorption of monoclonal IgGs and their F(ab')2 fragments onto polymeric surfaces, Colloids Surfaces B Biointerfaces. 5 (1995) 11–23. https://doi.org/10.1016/0927-7765(95)98205-2.

[33] B. Šustrová, K. Štulík, V. Mareček, P. Janda, A study of the modification of the gold electrode surface with a calix[4]arene self-assembled monolayer, Electroanalysis. 22 (2010) 2051–2057. https://doi.org/10.1002/elan.201000065.

[34] J. Leva-Bueno, S.A. Peyman, P.A. Millner, A review on impedimetric immunosensors for pathogen and biomarker detection, Med. Microbiol. Immunol. 209 (2020) 343–362. https://doi.org/10.1007/s00430-020-00668-0.

[35] S. Deb, A.A. Reeves, S. Lafortune, Simulation of physicochemical and pharmacokinetic properties of vitamin d3 and its natural derivatives, Pharmaceuticals. 13 (2020) 1–16. https://doi.org/10.3390/ph13080160.

[36] S. Zelzer, W. Goessler, M. Herrmann, Measurement of vitamin D metabolites by mass spectrometry, an analytical challenge, J. Lab. Precis. Med. 3 (2018) 99–99. https://doi.org/10.21037/jlpm.2018.11.06.

[37] G. Contreras Jiménez, S. Eissa, A. Ng, H. Alhadrami, M. Zourob, M. Siaj, Aptamer-based label-free impedimetric biosensor for detection of progesterone, Anal. Chem. 87 (2015) 1075–1082. https://doi.org/10.1021/ac503639s.

[38] A. Pyka, Evaluation of the lipophilicity of fat-soluble vitamins, J. Planar Chromatogr. - Mod. TLC. 22 (2009) 211–215. https://doi.org/10.1556/JPC.22.2009.3.10.

[39] D. Enko, G. Kriegshäuser, R. Stolba, E. Worf, G. Halwachs-Baumann, Method evaluation study of a new generation of vitamin D assays., Biochem. Medica. 25 (2015) 203–212. https://doi.org/10.11613/BM.2015.020.

[40] D. Chauhan, P.R. Solanki, Hydrophilic and Insoluble Electrospun Cellulose Acetate Fiber-Based Biosensing Platform for 25-Hydroxy Vitamin-D3 Detection, ACS Appl. Polym. Mater. 1 (2019) 1613–1623. https://doi.org/10.1021/acsapm.9b00179.

[41] D. Chauhan, A.K. Yadav, P.R. Solanki, Carbon cloth-based immunosensor for detection of 25-hydroxy vitamin D3, Microchim. Acta. 188 (2021) 145. https://doi.org/10.1007/s00604-021-04751-y.

[42] D. Chauhan, P.K. Gupta, P.R. Solanki, Amine Functionalized Noble Metal: Metal Oxide Nanohybrid for Efficient Electrochemical Determination of 25-Hydroxy Vitamin-D_3 in Human Serum, J. Electrochem. Soc. 168 (2021) 117508. https://doi.org/10.1149/1945-7111/ac3116.

[43] T. Sarkar, H.B. Bohidar, P.R. Solanki, Carbon dots-modified chitosan based electrochemical biosensing platform for detection of vitamin D, Int. J. Biol. Macromol. 109 (2018) 687–697. https://doi.org/10.1016/j.ijbiomac.2017.12.122.